Journal of ELECTRONIC MATERIALS, Vol. 44, No. 11, 2015
DOI: 10.1007/s11664-015-3956-5

Transition Metal–MoS_2 Reactions: Review and Thermodynamic Predictions

A.C. DOMASK,[1] R.L. GURUNATHAN,[1] and S.E. MOHNEY[1,2]

1.—Department of Materials Science and Engineering, The Pennsylvania State University, University Park, PA 16802, USA. 2.—e-mail: sem2@psu.edu

Molybdenum disulfide is a layered transition-metal dichalcogenide semiconductor that is attracting renewed attention for its potential use in future nanoscale electronics, optoelectronics, catalysis, tribology, and other fields. In all of these cases, the interaction between MoS_2 and various transition metals is very important. In this work we survey the thermodynamics of the metal–Mo–S systems and the anticipated reaction products from transition metals and MoS_2. We examined over 200 references on the reactions between transitions metals (M) and MoS_2, compiled thermodynamic data, and used the thermodynamic data to predict M–Mo–S ternary phase diagrams for systems without experimentally determined diagrams. Where possible, experimental literature on the interactions between metals and MoS_2 was used to corroborate our predicted diagrams and stable reaction products. Both the previously reported and newly predicted M–Mo–S phase diagrams fall into three categories. In the first category, the metal is in thermodynamic equilibrium with MoS_2. In another, there is a driving force for the metal to reduce MoS_2, with tie lines to sulfides of the contact metal dominating the phase diagram. In a final category, there is a very stable solid solution or ternary phase that dominates the phase diagram. Better understanding of the phase equilibria in the M–Mo–S systems will aid research on the use of MoS_2 in a variety of fields.

Key words: Molybdenum disulfide, two-dimensional material, van der Waals solid, dichalcogenide, phase equilibria, contact

INTRODUCTION

Molybdenum disulfide is a prototypical layered transition-metal dichalcogenide (TMD) in which interest has recently been renewed with the (re)discovery that a single layer can be isolated and used for a wide variety of purposes.[1,2] Researchers in areas as varied as electronics,[3–6] optoelectronics including photovoltaics,[7–9] tribology (lubrication),[10–12] catalysis,[13–15] and others are interested in MoS_2. Reduced dimensionality results in a number of unusual properties.

Single-layer MoS_2 has an intrinsic direct bandgap of around 1.8 eV,[16,17] which changes with increased layer number to an indirect bandgap of 1.20 eV to 1.29 eV in the bulk.[18–22] The electronic properties and reduced dimensionality make single- or few-layer MoS_2 attractive for field-effect transistors that are largely immune to short-channel effects, have high on–off ratio, and have low switching voltage.[2,7,23] Additionally, the ability to control both the spin and valley polarization of electrons makes MoS_2 a material of interest for novel electronic devices.[24,25] MoS_2 is being researched for use in a variety of nanoscale optoelectronic devices, including sensors, photovoltaics, and others. In all of these applications, efficient transport of charge carriers between metal contacts and MoS_2 is essential for optimal device performance,[7–9] and research is ongoing.[3–5,26]

Tribology researchers are investigating a wide variety of nanoscale MoS_2–transition metal systems for coatings and solid-state lubricants to be used in different environments (high temperature, corro-

(Received April 29, 2015; accepted July 22, 2015; published online August 18, 2015)

sive, etc.).[10,12,27,28] The large direct bandgap of single-layer MoS_2 is ideal for the hydrogen evolution reaction,[29] so researchers want to combine various transition metals and nanoscale MoS_2 to create an optimized, high-surface-area catalyst.[13,30,31] Catalysis researchers are also looking at two-dimensional (2D) versions of existing hydrodesulfurization materials (MoS_2 with metals such as Ni and Co).[14,32]

In each of these applications, the interaction between MoS_2 and various metals is important because either that interaction alters the primary properties of the system (e.g., wear resistance, catalytic activity, etc.) or MoS_2 is in contact with a metal, and the properties of all phases at the interface are important (e.g., electrical contacts). Essential to all of this work is knowledge of the reaction products resulting from the interaction between MoS_2 and various metals (M). The results in this paper and most of the existing literature reflect bulk systems. While the thermodynamics can be different in systems with reduced dimensionality, knowledge of interactions in bulk systems can inform future research on the nanoscale.

A few papers have experimentally investigated and/or predicted products resulting from the reaction between metals and MoS_2. Lince et al. performed an experimental study of the reaction between a subset of transition metals (M = Ag, Au, Co, Fe, Mn, Pd, Rh, Ti, and V) and the bulk MoS_2(0001) basal plane using x-ray photoelectron spectroscopy (XPS).[33] They also compared their experimental results with free energy of formation data for some of the metal sulfides that could form, to see whether reduction of MoS_2 was thermodynamically favored. Similar to the study by McGilp et al. detailed below, they did not consider the formation of all possible low-temperature metal sulfides, but only an abbreviated list. In addition, some of their experiments were complicated by oxidation of the metals, particularly Ti.

Other groups have attempted to use thermodynamic data to predict reactions between metals and MoS_2. McGilp et al. used thermodynamic data to predict the likelihood of reactions between various metals and a number of semiconductors including MoS_2.[34,35] The main shortcoming of their work was that they considered only one seemingly arbitrary M–S phase as the reaction product in each M–MoS_2 system, ignoring all other stable M–S or M–Mo phases. As a result, we came to different conclusions about some systems. Lastly, they did not look at all of the transition metal–MoS_2 systems, but instead looked only at M = Ag, Au, Co, Cu, Fe, Mn, Ni, Rh, Ti, and V.

EXPERIMENTAL PROCEDURES

This study combined thermodynamic calculations with existing experimental literature on reactions to learn as much as possible about transition metal–MoS_2 interactions. First, the various structures of MoS_2 are presented. Second, this study describes both the source of the thermodynamic data and the methodology used to calculate the ternary phase diagrams. Lastly, this work shows the three phase diagram types found in the M–MoS_2 systems.

Molybdenum Disulfide Crystallography

Within a single layer, the Mo–S bonds are strongly covalent (as evidenced by the short Mo–S distance), while adjacent layers are held together through much weaker, van der Waals forces, resulting in a van der Waals solid.[36]

In the bulk, MoS_2 has two common polymorphs: 2H-MoS_2 and 3R-MoS_2, the difference between them being the stacking order of S–Mo–S sheets. In both structures, Mo has trigonal-prismatic coordination.[36] 2H-MoS_2 has a hexagonal structure in space group $P6_3/mmc$ and ABABAB stacking order, while 3R-MoS_2 has a rhombohedral structure in space group $R3m$ and ABCABC stacking order.[36,37] The 3R-MoS_2 structure is metastable, and will transform to 2H-MoS_2 upon annealing at 873 K for around 3 weeks.[38] Most experimental research has been performed on 2H-MoS_2 bulk samples before work began on 2D samples, so unless otherwise noted, all literature summarized below was performed on bulk samples of the 2H-MoS_2 polymorph.

Source of Thermodynamic Data

This study used published thermodynamic data to calculate an isothermal ternary M–Mo–S phase diagram for about half of the transition-metal systems, while the other systems were excluded for the reasons below. In total, 25 M–Mo–S transition-metal systems are discussed herein. We present as much relevant literature for each system as could be found, as well as a ternary phase diagram where possible.

Lanthanum was excluded from the set of transition metals because there is very limited data for the La–Mo–S system and because it is often grouped in the lanthanide series rather than with the transition metals. Group 12 metals (Zn, Cd, and Hg), while *d*-block metals, are not considered transition metals in this study because they have filled *d* orbitals.[39] Additionally, they are less likely to be used in MoS_2-based devices because they have very low melting temperatures and, in the case of Cd and Hg, are toxic.

The Ag, Co, Cr, Hf, Nb, Ni, Re, Ta, Ti, and V systems have reported M–Mo–S ternary phases that are potentially stable at moderate temperatures: $AgMo_4S_5$,[40,41] $AgMo_6S_8$,[42] $CoMo_2S_4$,[43–46] $CoMo_3S_4$,[40,47] $CrMo_2S_4$,[43,46,48] $Cr_{1.5}Mo_6S_{7.7}$,[49] Hf_9Mo_4S,[50] $Nb_3Mo_2S_{10}$,[51] $NbMo_6S_8$,[52] $Nb_{20}Mo_{21}S_{59}$,[53] $NiMo_3S_4$,[47,54] $Re_4Mo_2S_8$,[55] $TaMoS_4$,[56] Ta_5MoS_{10},[57] Ta_9MoS_{18},[57] $TiMoS_3$,[58] $Ti_3Mo_3S_8$,[58] $Ti_{12}Mo_3S_{20}$,[58] $Ti_{20}Mo_{20}S_{60}$,[58] and VMo_2S_4.[43,46]

There are no thermodynamic data available for most of the above ternary phases, so phase diagrams were not calculated. Additionally, the Cu and Fe systems both have ternary phases, but published phase diagrams show those phases unstable at temperatures below 873 K. It is unknown whether the ternary phases listed above are stable at low temperatures.

An additional issue to note is the possibility for transition-metal intercalation into MoS_2, whereby a transition-metal atom diffuses into the van der Waals gap in either an ordered or disordered fashion. This behavior is more energetically favored in other TMDs such as NbS_2 and TaS_2, but it also occurs in MoS_2.[59] The filled d_{z^2} band of Mo in MoS_2 makes accommodating transition-metal species in the van der Waals gaps more difficult because any electron transfer must occur into the higher energy bands. Additionally, the interstitial site in MoS_2 is smaller than the ones in TaS_2 and NbS_2 as a result of their crystal structures, making interstitial accommodation of transition-metal atoms less energetically favorable.[60] As a result, on intercalation, the structure of the individual MoS_2 sheets is often distorted to make additional room in the van der Waals gap.

The ternary M–Mo–S phases can be grouped into four basic categories: MoS_2 intercalates, Mo_6S_8 Chevrel-based structures, structures based on other TMDs, and other.

$CoMo_2S_4$,[44] $FeMo_2S_4$,[44] $CrMo_2S_4$,[43] and V_2MoS_4[61] all display relaxed, MoS_2-based structures, where the metal atoms sit in interstitial spaces. In VMo_2S_4, both the V and Mo are found on both the metal sublattice sites and the interstitial sites.[61] In $Ti_3Mo_3S_8$ and in lightly Nb-doped MoS_2, the metals substitute for the Mo on the metal sites and no atoms are found at the interstitial sites.[58,62] Also known or suspected to intercalate are Pd and Ni[63] and Fe when MoS_2 is not sulfur enriched.[64]

The Chevrel phases have a structure of long, one-dimensional Mo_3S_4 chains alongside transition-metal clusters, often with varied occupancy fractions. Mo_3S_4 alone can only be formed by first creating a Chevrel phase and then etching away the second metal; when heated, it decomposes.[65]

Many ternary phases are Chevrel phases, including $CoMo_3S_4$, $NiMo_3S_4$, $Fe_xMo_3S_4$,[47] $AgMo_4S_5$,[40] $AgMo_6S_8$,[42] $Re_4Mo_2S_8$,[55] $Cu_{1.8}Mo_6S_8$,[66] $Cu_{2-x}Mo_3S_4$,[67] $FeMo_{4.12}S_6$,[68] and $TiMoS_3$.[58] Additionally, while the crystallographic information was incomplete, the cited authors believed that $NbMo_6S_8$ is also of this structure type.[52]

Structural similarities between MoS_2 and the disulfides of Nb and Ta result in a number of ternary structures based on their various layered geometries. The metal atoms in each either substitute on the primary metal lattice or occupy interstitial spaces in the van der Waals gaps. $TaMoS_4$, Ta_5MoS_{10}, Ta_9MoS_{18}, and $Nb_3Mo_2S_{10}$ are examples of these types of layered phases.[51,56,57] In the "other" category are Hf_9Mo_4S,[58,69] $Ti_{12}Mo_3S_{20}$, and $Ti_{20}Mo_{20}S_{60}$[58] with unrelated structures, and $Nb_{20}Mo_{21}S_{59}$, $Cr_{1.5}Mo_6S_{7.7}$, and $FeMo_5S_6$ with incomplete crystallographic information.[47,49,53]

The systems for which thermodynamic data were compiled and used to calculate a ternary phase diagram are M = Mn, Fe, Ru, Os, Rh, Pd, Pt, Cu, and Au. The binary M–Mo and M–S phase diagrams served as the source for the definitive list of stable, low-temperature binary intermetallic compounds. *Binary Alloy Phase Diagrams*[70] and other literature sources were used, and all sources are cited in the specific sections below.

Solid solubility is not treated in our calculations, and intermetallic phases were treated as line compounds. Where there may be solubility of a transition metal in MoS_2 but its extent is not known or not great, we treat MoS_2 as a line compound.

This study ignored the vapor pressure of S_2 above MoS_2 because thermodynamic calculation determined that it is negligible at temperatures of interest for this work and because Brainard did not experimentally detect dissociation of MoS_2 below 1200 K in vacuum.[71]

In order to calculate a ternary phase diagram, the enthalpy of formation (ΔH_f°) and entropy of formation (ΔS_f°) for each of the equilibrium phases are required. The majority of these data are from two sources: *Materials Thermochemistry* by Kubaschewski and *Cohesion in Metals: Transition Metal Alloys* by de Boer.[72,73] Additional sources for thermodynamic data used in this study are cited in the sections below. See Appendix Table I for a table of the data used. For the eight M–Mo phases for which ΔH_f° could not be found, Miedema's estimate was used (as tabulated in de Boer).[73,74]

Experimental data for ΔS_f° were available for most of the binary intermetallic compounds considered. When it could not be found, ΔS_f° was assumed to be zero. This approximation is reasonable given that all of the phase transitions in this work are solid-phase reactions; therefore, the change in entropy on reaction is small when compared with the change in enthalpy.

Of particular importance in every diagram are the values ΔH_f° and ΔS_f° for MoS_2. Used in this study were $\Delta H^\circ_{f,MoS_2} = -91.9$ kJ/(mol of atoms) and $\Delta S^\circ_{f,MoS_2} = -10.0$ J/(K·mol of atoms), the values tabulated by Kubaschewski.[72] These thermodynamic values for MoS_2 are also within the stated error of those presented in the latest NIST WebBook.[75]

Using all the gathered data, the Gibb's energy of formation (ΔG_f°) for each stable, low-temperature binary compound was calculated for 298 K, using

$$\Delta G_f^\circ = \Delta H_f^\circ - T\Delta S_f^\circ, \quad (1)$$

and can be found tabulated in Appendix Table I.

Ternary Diagram Calculation

The overall process for predicting ternary phase diagrams is (1) determine all possible tie lines in a system, (2) calculate ΔG°_{rxn} per atom for each equation to determine the favored pair of phases, and (3) draw a ternary phase diagram reflecting the favored pairs of phases, as in the work by Schmid-Fetzer and others.[76,77] A program was written in MATLAB version R2014a to automate this process.

Solid tie lines in the ternary phase diagrams indicate the most energetically favored diagram. When the absolute value of ΔG°_{rxn} was calculated and found to be less than 8 kJ/(mol of atoms) for a set of compounds, the alternative diagram is indicated by dashed lines.[77] Alternative diagrams were found in the Fe, Rh, and Pt systems.

Published ternary phase diagrams were presented mostly for 773 K (Cu, Fe, and W systems), although the Ti diagram was for 1573 K and the V diagram was for 1373 K. Given the solid-state nature of this work and therefore the limited entropic contribution to the overall free energies of formation, it is not unreasonable to assume that a diagram established for a moderate temperature will be similar to one drawn for room temperature. However, one should also note that, in some cases, the stable binary sulfides at an elevated temperature are not the same sulfides that are stable at room temperature, and therefore those diagrams must differ.

Ternary Phase Diagram Types

Both the previously reported and calculated M–Mo–S phase diagrams fall into three categories. In the first category, the metal and all binary phases are in thermodynamic equilibrium with MoS_2, being termed MoS_2 dominant. In the next, there is a driving force for the metal to reduce MoS_2, with tie lines to very energetically favored sulfides of the contact metal dominating the phase diagram, being termed metal-sulfide dominant. In the final category, there is a very stable solid solution or ternary phase that dominates the phase diagram, being termed solid solution/ternary phase dominant. The term "dominant" used here means the tie lines converge to a particular phase. Figure 1 depicts graphically which diagram type was found for each M–Mo–S system.

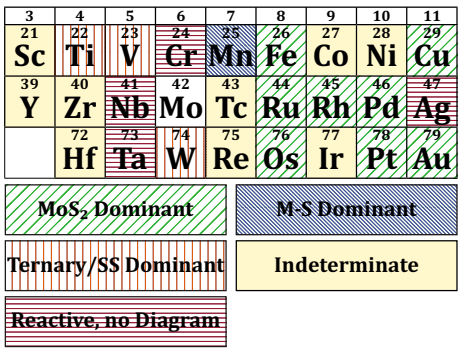

Fig. 1. Periodic table depicting the type of M–Mo–S ternary phase diagram for each of the transition metals. Ternary phase diagrams were calculated at room temperature for all systems labeled "MoS_2 Dominant" and "M–S Dominant." The systems noted as "Ternary/Solid Solution Dominant" have existing ternary phase diagrams published in the literature at various temperatures: Ti (1573 K),[58] V (1373 K),[61] and W (773 K).[78] The systems labeled as "Indeterminate" lacked sufficient existing thermodynamic data and experimental literature for any conclusions to be drawn. The systems described as "Reactive, no Diagram" are systems where experimental literature exists describing reactivity at moderate temperatures, but we could not calculate a ternary phase diagram.

MoS_2 Dominant Diagrams

This ternary phase diagram reflects the thermodynamic equilibrium and resulting tie line between the transition metal and MoS_2. As a result, no new phases will form on the interaction between M and MoS_2. A schematic of this type of diagram can be seen in Fig. 2. The ternary systems of this type are all in groups 8 to 11, including the group 8 metals Fe, Ru, and Os; the group 9 metal Rh; the group 10 metals Pd and Pt; and the group 11 metal Au. Cu also adopts this diagram type per our calculations for room temperature, although the published diagram for 773 K does not.

Metal-Sulfide Dominant Diagrams

The diagrams in this category—those for Mn and Cu (at 773 K)—all have a stable metal-sulfide compound that is dominant, as can be seen in Fig. 3. In no system did this study find a dominant M–Mo phase.

Solid Solution or Ternary Phase Dominant Diagrams

In three systems (W, V, and Ti), previously published ternary diagrams are dominated by either a solid solution or a ternary phase—W in the former case and Ti and V in the latter. Since no general schematic diagram can be drawn, further informa-

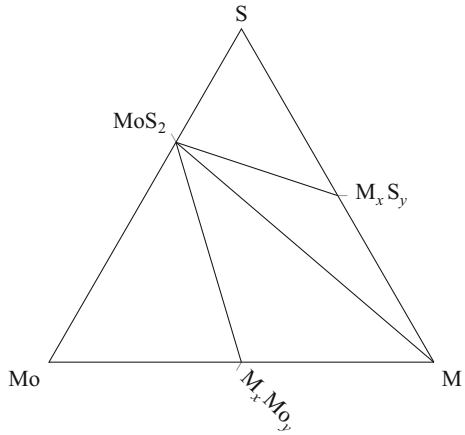

Fig. 2. MoS_2-dominant phase diagram showing the equilibrium between the transition metal M and MoS_2.

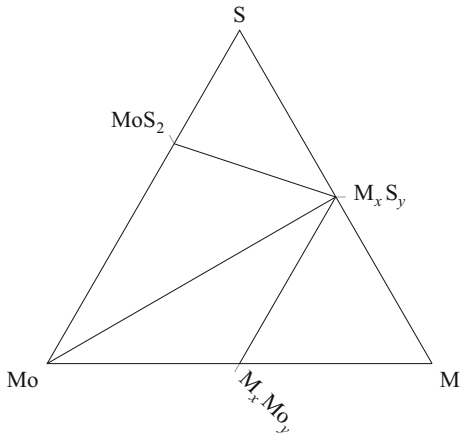

Fig. 3. Metal-sulfide dominant phase diagram showing the tie lines emanating from a metal sulfide to both MoS_2 and Mo metal, as well as a M–Mo phase.

tion about those systems is presented individually below.

RESULTS

Below is a description of each system studied, along with either a previously published or a calculated phase diagram where possible. Diagrams determined by this study are compared with experimental studies of the reactions from the literature, typically corroborating the proposed diagrams. Where a phase diagram cannot be presented, a review of the literature pertaining to reactions is still presented since it also sheds light on the types of and kinetics of the reactions. The elements are presented by group to reveal systematic trends across the periodic table.

Group 3: Sc and Y

Scandium The binary Sc–S diagram is not available. Three phases (Sc_2S_3, $Sc_{1.37}S_2$, and ScS) are known, although thermodynamic data are only available for the second.[79] There are no binary Sc–Mo intermetallic compounds.[80] Survey of the literature found no reported Sc–Mo–S ternary phases and no experimental results. Given the limited data available, no diagram was calculated.

Yttrium No binary phases are shown on the Y–Mo phase diagram.[81] Three Y–S phases have been reported in the literature (YS, Y_5S_7, and YS_2), but no binary phase diagram is available.[82] Insufficient thermodynamic data are available to calculate a ternary phase diagram in the Y–S–Mo system. Additionally, no experimental literature on this ternary system could be found.

Group 4: Ti, Zr, and Hf

Titanium A partial Ti–Mo–S ternary phase diagram for 1573 K was published by Wada et al. and includes the ternary phases $TiMoS_3$, $Ti_3Mo_3S_8$, $Ti_{12}Mo_3S_{20}$, and $Ti_{20}Mo_{20}S_{60}$.[58] All four ternary phases show a range of homogeneity. The binary Ti–Mo system shows no intermetallic phases.[83] In the Ti–S binary system, there is a layered and a one-dimensional (1D) transition-metal chalcogenide, TiS_2 and TiS_3, respectively,[37] and many other titanium sulfides. Ti is not in equilibrium with MoS_2. Various studies have reported high reactivity between Ti and MoS_2, driven by strong reactivity between Ti and S.[33,37,84] Ti films on MoS_2 reacted on deposition without annealing.[37] However, more studies that perform thorough materials characterization are needed to understand the reactions in detail.

Zirconium There is one intermetallic phase ($ZrMo_2$) in the Zr–Mo system[85] and several reported zirconium sulfides.[86]

Umarji et al. mentioned in a footnote that they had synthesized the Zr–Mo–S ternary compound $Zr_{1.2}Mo_6S_8$ and would describe it in further detail in a future publication.[42] Unfortunately, this follow-up publication could not be found. Since all of the metals surrounding Zr in the periodic table form ternary phases, it is likely that Zr will as well. Therefore, Zr has been classified as an unknown phase diagram type.

If the ternary phase is ignored, the resulting calculated diagram is Zr_3S_4 dominant.[85–87] No existing literature could be found on the interaction between Zr and MoS_2, so the predicted phase diagram could not be corroborated.

Hafnium A binary Hf–S phase diagram is not available, although $Hf_{\sim 5}S$, Hf_2S, HfS, Hf_3S_4, HfS_2, and HfS_3 are reported in the literature.[88] The Hf–Mo binary phase digram has only one low-temperature intermetallic phase ($HfMo_2$).[89] The ternary phase Hf_9Mo_4S has also been observed and formed readily after 6 h to 24 h at 1850 K.[69] HfS_2 is a layered TMD similar to MoS_2.[37,69] Both HfS_2 and HfS_3 are very stable phases, with free energies of formation for 298 K that are well below that of MoS_2 [−192 kJ/(mol of atoms) and −189 kJ/(mol of atoms), respectively].[90] No experimental research could be found regarding the interaction between Hf and MoS_2. Given the above information, it can be hypothesized that the ternary phase diagram will not likely be MoS_2 dominant, and instead will be dominated either by one of the Hf–S phases or by Hf_9Mo_4S.

Group 5: V, Nb, and Ta

Vanadium While some ambiguity exists in the published V–Mo–S ternary phase diagrams experimentally derived for 1373 K by Wada et al., the diagram is dominated by the $V_{1+x}Mo_{2-x}S_4$ ($0 \leq x \leq 2$) ternary solid solution.[61] On one end of this composition line is V_3S_4,[91] a layered chalcogenide, and on the other is the terminal composition VMo_2S_4.[43,46] Powell et al. and others have carefully explored this solid solution phase to better under-

stand a change in the resistivity, whereby a more V-rich material is metallic, while a more Mo-rich phase is semiconducting.[92] This system is characterized as solid solution dominant.

Niobium and Tantalum Nb and Ta have similar interactions with Mo, S, and MoS_2, and therefore will be addressed together. Both Nb and Ta form a solid solution with Mo.[93] Nb and Ta form a number of stable sulfides,[94,95] and each forms three ternary M–Mo–S intermetallic compounds ($Nb_3Mo_2S_{10}$,[51] $NbMo_6S_8$,[52] $Nb_{20}Mo_{21}S_{59}$,[53] $TaMoS_4$,[56] Ta_5MoS_{10},[57] and Ta_9MoS_{18}[57]). Both elements form a transition-metal disulfide (NbS_2 and TaS_2) with a layered structure similar to MoS_2. The quasibinary systems between MoS_2 and both TaS_2 and NbS_2 include a number of layered phases.[51,57,96]

NbS_2 has a $\Delta G_f^\circ = -149.30$ kJ/(mol of atoms) at 1123 K to 1373 K, compared with −79.2 kJ/(mol of atoms) for MoS_2 at 1273 K.[97] Similarly stable is TaS_2 with $\Delta G_f^\circ = -122$ kJ/(mol of atoms) at 298 K.[72] The quasibinary phase diagram between both NbS_2 and TaS_2 and MoS_2 each contains multiple ternary phases with ranges of solubility.[51,57] While there is not enough information to draw a ternary phase diagram in either system, it is anticipated that both Nb and Ta are favored to react with MoS_2 at moderate temperatures if kinetics will allow.

Group 6: Cr and W

Chromium The Cr–S binary diagram shows eight low-temperature intermetallic phases, while the Cr–Mo system has a large miscibility gap but no intermetallic phases.[98,99] A partial ternary phase diagram for 1273 K is available for this system, and shows two stable ternary phases: the monoclinic phase $CrMo_2S_4$ and the triclinic phase of approximate stoichiometry $Cr_{1.5}Mo_6S_{7.7}$.[43,49] The ternary phase $Cr_{1.4}Mo_6S_{7.5}$ can be formed at temperatures as low as 458 K. Apart from the research into these two ternary phases, two studies could be found investigating the interaction between Cr and MoS_2.

When a very thin film of Cr (1.8 nm and 3.4 nm) was deposited on MoS_2(0001), reaction was observed both on deposition and as the result of annealing.[100,101] After thermal evaporation, the Cr reduced a small amount of the MoS_2 and incorporated about 1% S into the metallic Cr layer and formed a more sulfur-rich surface layer (~5%). One or more chromium sulfides were detected via XPS. The study did not determine exactly which phases were formed, nor did it consider the formation of a ternary phase, but most of the Cr was metallic. At the interface between the Cr and MoS_2, a metallic Mo layer was formed.

After annealing at temperatures ≤823 K, the Cr layer incorporated more S, and the metallic Mo interfacial layer thickened. As the temperature was increased from 823 K to 923 K, more of the Cr metal reacted with sulfur, producing chromium sulfide(s), although the bulk of the chromium remained metallic. No annealing times were given.

The limited phase diagram by Oshima et al.[49] and the experimental work by Durbin et al.[100,101] discussed above show that the full ternary diagram cannot be MoS_2 dominant. More research needs to be done to predict the equilibrium products between few-layer MoS_2 and excess Cr metal.

Tungsten Both W and Mo form very stable, layered TMDs with similar electronic properties (bandgaps that differ by less than 10%), the same structure, and lattice parameters that differ by less than 0.2% in the a lattice parameter and less than 0.6% in the c lattice parameter.[37,102] As a result, the W–Mo–S ternary phase diagram (in Fig. 4) for 773 K by Moh et al.[78] shows a complete ternary solid solution, $(W,Mo)S_2$, whereby tungsten and molybdenum interchangeably occupy the trigonally coordinated site and the sulfur remains in the pyramidal locations.[36]

At 773 K, MoS_2 is more stable, so the tie lines between the MoS_2–WS_2 solid solution and the Mo–W solid solution include a tie line between a very MoS_2-rich solution and tungsten-rich solution, as shown in Fig. 4. Therefore, interdiffusion is not expected between elemental W and MoS_2.

Group 7: Mn, Tc, and Re

Manganese There are only two room-temperature Mn–S and one Mn–Mo phases.[103,104] The Mn–S system has not been completely experimentally determined because of the low-temperature decomposition of MnS_2 and high reactivity with oxygen.[105] Thermodynamic values for MnS_2 from Ref. 105 were used to calculate Fig. 5. The value for the free energy of formation of Mn_5Mo_4 was taken to be −1 kJ/(mol of atoms) instead of using Miedema's estimate, because the estimate for the compound is +7 kJ/(mol of atoms); no data were available on the en-

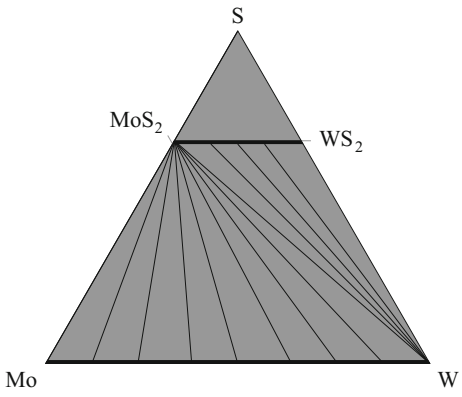

Fig. 4. W–Mo–S phase diagram for 773 K reproduced from Ref. 78. Black regions are single-phase regions, and gray regions are two-phase regions. Tie lines in the bottom half of the diagram do not divide adjacent phase fields, but instead indicate the dominant pair of phases at a particular composition.

tropy of formation, and the phase is accepted as stable on the binary phase diagram.

The sulfide, MnS, is dominant, so Mn reduces MoS_2. The calculated ternary phase diagram is consistent with experimental data. Lince et al. thoroughly studied the interaction between Mn and MoS_2 as a function of annealing temperature using XPS. They reported that, on deposition, some fraction of the Mn metal reacted to form various Mn–S phases.[106] On annealing to 770 K, the Mn–S/metallic Mo overlayer continued to grow, and S vacancies formed in the MoS_2 substrate (no annealing times were presented). Some of the Mn remained unreacted until annealing at higher temperatures (850 K to 1040 K). The study looked for and found no ternary Mn–Mo–S phases.

The experimental literature and our thermodynamic calculations agree that Mn and MoS_2 will react at moderate temperatures. This reaction results in a combination of MoS_2, MnS, Mo, Mn_5Mo_4, and Mn, depending on the ratio of elements that are present.

Technetium The Tc–Mo diagram is available,[107] but the Tc–S diagram is not available and thermodynamic data for those phases could not be found.[108] Also, no reports of experimentation in the Tc–Mo–S system are reported in the literature.

Rhenium A binary Re–Mo diagram has been published,[109] but no Re–S diagram exists. There is one known ternary phase (the Chevrel phase $Re_4Mo_2S_8$[55]).

Research into Re doping of MoS_2 revealed that Re inclusions (which are common in some natural molybdenite deposits) stabilize the 3R-MoS_2 polymorph.[38] Tiong et al. published a series of papers on the Re–MoS_2 reaction and found that the inclusion of very small amounts of Re (<1%) changed the stacking order of the S–Mo–S layers on formation at 1223 K, which stabilized the 3R-MoS_2 structure as opposed to the typical 2H-MoS_2 polymorph.[110] The substitution of Re^{4+} ions on the Mo^{4+} sites in the natural mineral molybdenite caused distortion of the structure.[111] Furthermore, for Re concentrations greater than 5%, growth of single-crystal Re-doped MoS_2 using chemical vapor deposition was no longer possible: a second phase was formed.[112] ΔG_f° for ReS_2 is −96.4 kJ/(mol of atoms) at 298 K,[97] which is slightly larger than the value for MoS_2 [−88.6 kJ/(mol of atoms)]. Additional research into the Re–Mo–S ternary system is necessary in order to understand the reaction products for different conditions.

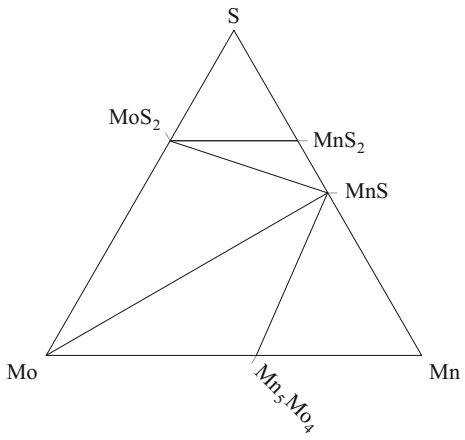

Fig. 5. Calculated Mn–Mo–S phase diagram for 298 K.

Group 8: Fe, Ru, and Os

Iron The Fe–Mo–S ternary phase diagram for various temperatures is presented in the work by Raghavan.[113] The ternary phase diagram for 773 K is MoS_2 dominant, as shown in Fig. 6. The only ternary intermetallic phase Raghavan included in his diagrams was $FeMo_4S_6$, which formed at 808 K.[68] Additionally, various other sources report ternary phases with the following stoichiometry (and multiple polymorphs in some cases): $FeMo_2S_4$,[43,44,46,114] $FeMo_{4.12}S_6$,[68] $Fe_xMo_3S_4$ with $x < 1$,[47] and $FeMo_5S_6$.[41] Raghavan stated in his book that "the present status of understanding of the ternary phases of this system is clearly not satisfactory and there is need for further study."[113]

The available experimental literature disagrees as to which binary or ternary intermetallic phases form upon the interaction between thin Fe films and MoS_2 at high temperatures.[33,63,115–117] However, none of the available literature reported reactivity between Fe and MoS_2 at or below 773 K, which is reflected in the published diagram (shown in Fig. 6).[113] (Our calculation of the Fe–Mo–S ternary phase diagram at 773 K agreed with the published diagram as MoS_2 dominant.)

The Fe–Mo–S diagram calculated for room temperature by this study also showed a MoS_2 dominant structure, although the diagram has some uncertainty reflected by the dashed (alternate) lines. However, the free energy of reaction for $MoS_2 + 4Fe \rightarrow FeS + Fe_2Mo$ [−7.4 kJ/(mol of atoms)] is barely less than our

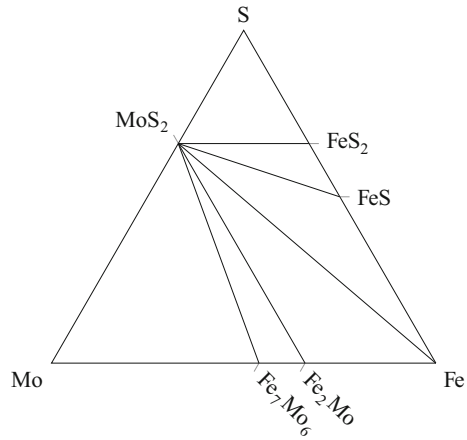

Fig. 6. Reproduction of Fe–Mo–S phase diagram by Raghavan[113] for 773 K.

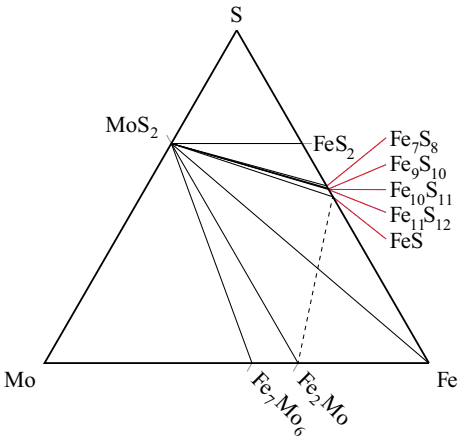

Fig. 7. Calculated Fe–Mo–S phase diagram for 298 K. Dashed lines indicate tie lines that are unstable by a narrow margin.

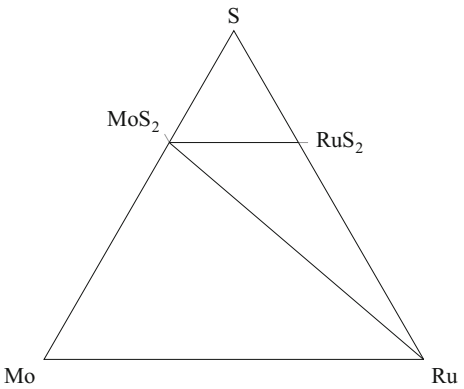

Fig. 8. Calculated Ru–Mo–S phase diagram for 298 K.

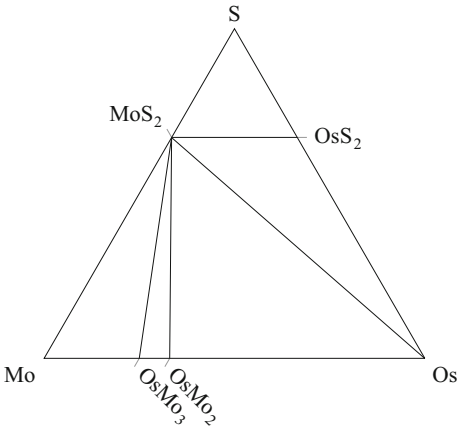

Fig. 9. Calculated Os–Mo–S phase diagram for 298 K.

threshold value [−8 kJ/(mol of atoms)] for acceptance without a caveat, and the thermodynamic values for all the compounds involved in that calculation are not estimations but instead are from the literature. The only difference between the room temperature and 773 K diagrams is the inclusion of four additional Fe–S phases that are not stable at 773 K, as shown in Fig. 7.[118] We do not expect the type of diagram to change between room temperature and 773 K.

Ruthenium and Osmium Phases from the relevant binary phase diagrams were used to calculate the two ternary phase diagrams shown in Figs. 8 and 9.[119–122] Unfortunately, this study found no literature on the interaction between MoS_2 and either Ru or Os, and therefore it was not possible to corroborate the calculated diagrams.

Group 9: Co, Rh, and Ir

Cobalt A number of Co–S and Co–Mo phases exist (CoS_2, Co_3S_4, Co_9S_8, Co_7Mo_6, and Co_3Mo).[123–125] Two ternary phases are known ($CoMo_2S_4$ and $CoMo_3S_4$) but are difficult to form.[41,46] If one ignores the two ternary phases and calculates a ternary phase diagram, the calculated diagram is MoS_2 dominant. We show no diagram because the temperatures at which the ternary phases are stable are not known.

No reaction between MoS_2 and Co has been seen below ~800 K in the experimental literature. Early literature found no reaction when an 80% Co–20% MoS_2 mixture was heated to a temperature of 1073 K.[126] In later studies, upon e-beam evaporation, one monolayer of Co was metallic and did not form Co–S bonds until annealed to 790 K; similarly, when deposited via pulsed laser, the adatoms had sufficient energy to remove some S from the MoS_2 surface, but the Co remained metallic.[127,128] The liberation of some S was postulated to be due only to the bombardment of the substrate with energetic species, as had been seen in earlier studies of Ar-ion bombardment of MoS_2.[129] In general, both studies found Co and MoS_2 to be unreactive at room temperature. This conclusion is consistent with the calculated free energy of formation at room temperature of the various Co–S phases—they are all greater than −50 kJ/(mol of atoms), which is much less negative than for MoS_2.

In both articles, on annealing at ~800 K for 3 min, metallic Mo formed, and the Co changed electronic configuration and had reduced metallicity. This indicated Co–S bonding, potentially forming CoS (a phase stable above 733 K).[123] Additionally, when annealed to high temperature, the Co-rich overlayer agglomerated, and uncovered metallic Mo. Therefore, Co is reactive with MoS_2 at higher temperatures, even though it may be unreactive near room temperature.

Rhodium The Rh–S and Rh–Mo binary phase diagrams both contain multiple low-temperature intermetallics.[130,131] The phase diagram seen in Fig. 10 was calculated using the sources described in the methodology section as well as an article specifically on Rh–S phases.[72,73,132] While included on some Rh–S phase diagrams, RhS_2 has been excluded in this work because there is controversy over its

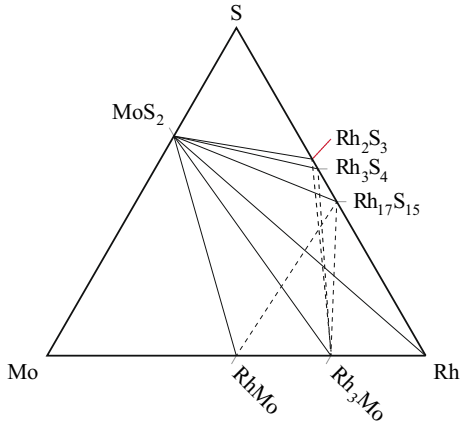

Fig. 10. Calculated Rh–Mo–S phase diagram for 298 K. Dashed lines indicate tie lines that are unstable by a narrow margin.

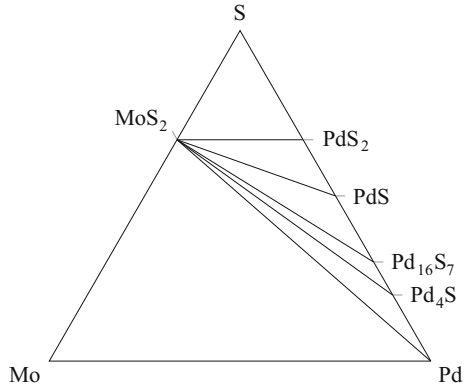

Fig. 11. Calculated Pd–Mo–S phase diagram for 298 K.

existence as a separate phase and because no thermodynamic data could be found.[132,133] A number of phases that are predicted to be unstable by only a narrow margin are presented as well, which, if stable, would result in diagrams with a number of different tie line configurations. This is because reactions of the form $MoS_2 + Rh_aS_b \rightleftharpoons Rh_cS_d + Rh_xMo_y$ have low free energies of reaction (positive or negative). The only experimental work that could be found on Rh–MoS_2 interactions reported no reaction between MoS_2 and Rh upon room-temperature deposition of a few to 10 nm of Rh.[33] Therefore, the Rh–Mo–S diagram is probably MoS_2 dominant, but it could have mixed dominance.

Iridium The binary Ir–S diagram is not available, the list of phases is not agreed upon, and the available Ir–Mo diagram does not contain any information below 1473 K.[134] This study could not find any reference of any Ir–Mo–S ternary phases, nor any experimental exploration of the ternary system in the literature. Additionally, thermodynamic data could not be found for many of the phases. Therefore, no phase diagram was calculated.

Group 10: Ni, Pd, and Pt

Nickel Both the Ni–S and Ni–Mo diagrams contain many binary intermetallic compounds (NiS_2, Ni_3S_4, NiS, Ni_9S_8, Ni_3S_2, Ni_2Mo, Ni_3Mo, Ni_4Mo, Ni_8Mo at room temperature).[135,136] A ternary Chevrel solid solution phase also exists, $Ni_2Mo_6S_8$.[54,137] Insufficient data were available to calculate a ternary phase diagram.

Multiple studies have seen no reaction of Ni upon deposition onto MoS_2.[138,139] Of particular note is the study by Papageorgopoulos, where a Ni-coated MoS_2 film was annealed for 2 min at a variety of temperatures. Below 600 K, no interaction between the two materials was detected. Between 600 K and 800 K, they saw evidence of partial Ni diffusion into MoS_2, while at higher temperatures, they saw agglomeration of the remaining surface Ni and continued diffusion of the Ni within the MoS_2. Further work by this group looked at Auger depth profiles of Ni-coated MoS_2. Each cycle consisted of a few monolayers of Ni metal being deposited and the sample being heated to 1200 K for a few minutes. That deposition/annealing cycle was repeated 20 times. The depth profiling showed no significant variation in Ni concentration as a function of depth: the Ni diffused evenly through the MoS_2 within the thickness they probed[63] and may have intercalated.

Palladium The binary phase diagrams along with the thermodynamic data sources mentioned above and the work by Zubkov et al. on Pd–S compounds were used to calculate the ternary Pd–Mo–S diagram shown in Fig. 11.[140–142] The diagram calculated in this study found palladium metal as well as a number of palladium sulfide compounds in equilibrium with MoS_2 and, therefore, a MoS_2 dominant diagram. The lack of reaction between palladium and MoS_2 predicted by this study is reflected in the literature.

A number of studies of very thin Pd layers atop both single-layer and bulk MoS_2 found no reaction: in the former case, 2 nm of Pd was found to fully wet but not react with a single-layer substrate upon deposition, and, in the latter, deposition of extremely small quantities (less than a monolayer) of Pd at 493 K formed epitaxial clusters.[26,143]

Kamaratos et al.[63] studied the diffusion of Pd at high temperatures through MoS_2 in the *c*-direction, and found that it intercalated between the S–Mo–S layers. They induced this effect by first depositing a few monolayers of Pd on the MoS_2(0001) surface and then heating to high temperatures (1200 K) for 20 min. This heat treatment was repeated 20 times. The depth to which Pd diffused was not established, but the concentration smoothly decreased with penetration depth in the *c*-direction. They used this information to report the lack of formation of any Pd-based intermetallic phases and assumed the Pd intercalated, although their application of Auger

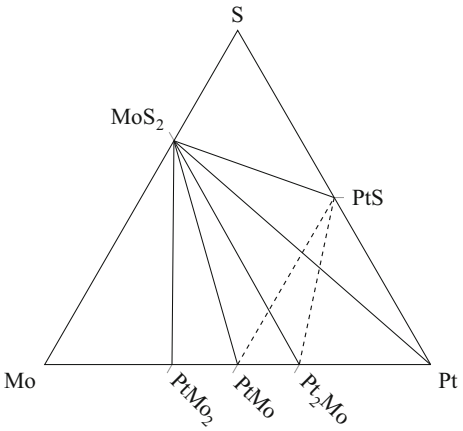

Fig. 12. Calculated Pt–Mo–S phase diagram for 298 K. Dashed lines indicate tie lines that are unstable by a narrow margin.

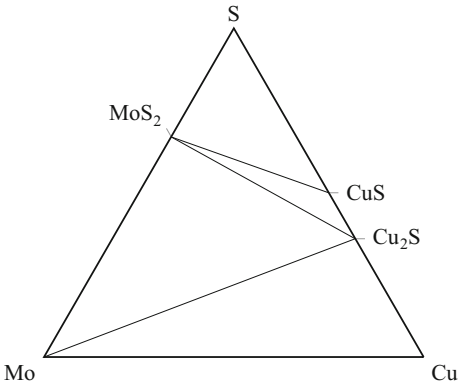

Fig. 13. Cu–Mo–S phase diagram for 773 K, reproduced from Huang et al.[148] The phase noted as Cu_2S is actually a cubic solid solution ranging from Cu_2S to $Cu_{1.8}S$.

electron spectroscopy cannot conclusively confirm that claim.

Platinum Both Pt–S and Pt–Mo binary intermetallic compounds exist.[144,145] Our calculations show that four Pt–Mo and a Pt–S phases, as well as metallic platinum, are in equilibrium with MoS_2, resulting in Fig. 12. There is some uncertainty in the Pt–Mo–S system; therefore, the dashed lines indicate a less likely Pt–Mo–S diagram that has mixed dominance.

The calculated equilibrium between MoS_2 and Pt is consistent with the literature. Hofmann et al. studied the deposition of thin-film MoS_2 onto bulk Pt metal by metalorganic chemical vapor deposition. Inert gas carried H_2S and $Mo(CO)_6$ for deposition onto Pt heated to 623 K. The study reported no reaction between the two, and incomplete coverage of the Pt by MoS_2, but they performed limited characterization.[146] Similarly, Pt electrochemically deposited on MoS_2 agglomerated.[147] XPS of the surface detected signal for Pt and MoS_2 but no other phases, suggesting a lack of reaction.

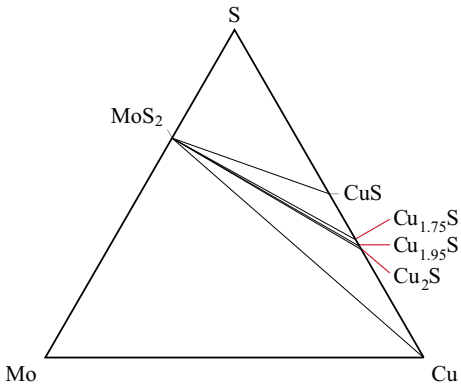

Fig. 14. Calculated Cu–Mo–S phase diagram for 298 K.

Group 11: Cu, Ag, and Au

Copper The Cu–Mo–S ternary phase diagram has been explored at and above 773 K.[148] At 773 K, the diagram is dominated by Cu_2S as seen in Fig. 13, but the diagram for 873 K shows the ternary phase $Cu_xMo_3S_4$ with a wide phase field in Cu, Mo, and S.[137,148,149] Cu_2S, the dominant Cu–S phase at 773 K, is not stable below 348 K;[150] therefore, the phase diagram shown in Fig. 13 cannot reflect the equilibrium ternary phase diagram for room temperature.[150–152] On trying to reproduce the 773 K Cu–Mo–S diagram, a MoS_2 dominant diagram was calculated, in contrast to the Cu_2S dominant diagram found in the literature. However, the Gibbs free energies of reaction are very small when comparing competing tie lines.

We also calculated the Cu–Mo–S ternary phase diagram for room temperature and found that it is not metal-sulfide dominant; it is predicted to be MoS_2 dominant, as can be seen in Fig. 14.[150,152,153] Given the dramatically different diagrams at 773 K and 298 K and the large number of stable phases and invariant reactions seen in this system at moderate temperatures, additional study is necessary to determine the equilibrium phases at other temperatures.

Silver Only one Ag–S binary compound exists (Ag_2S), and there are no intermetallic phases and low miscibility in the Ag–Mo system.[154,155] Two Ag–Mo–S ternary compounds have also been reported—$AgMo_4S_5$ and $AgMo_6S_8$[40–42]—and therefore a ternary phase diagram could not be calculated for this system.

The earliest studies in this system saw no reaction in a mixture of 20% Ag in MoS_2 up to the melting point of Ag.[126] Work by Souder et al. in 1971 used a radioactive tracer to show the diffusion of Ag into MoS_2 on annealing. At temperatures of 673 K to 873 K for 5 min, they reported that the Ag diffused into spaces between the MoS_2 layers but found no detectable diffusion in the lateral direction (parallel to the layers).[156] The study did not try to determine the stoichiometry or crystal structure of any resulting phases.

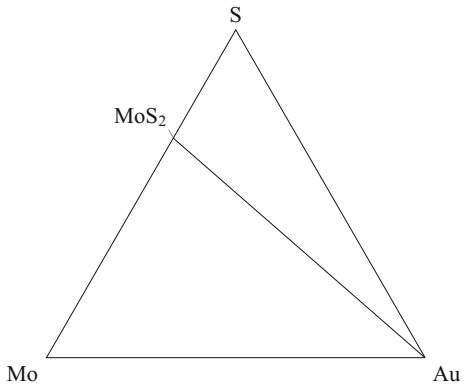

Fig. 15. Calculated Au–Mo–S phase diagram for 298 K.

Li et al. performed the most comprehensive study of the interaction between Ag and MoS_2 as a function of temperature. When deposited at temperatures below 300 K, Ag did not react with MoS_2. On annealing to 400 K (no time given), Ag diffused into MoS_2, forming what they called $AgMoS_x$, a "probably amorphous bimetal sulfide." This phase decomposed at around 800 K, forming Ag clusters, which then desorbed from the surface at ~850 K, leaving behind MoS_2.[157] Given the experimental research, the Ag–Mo–S system is described as reactive because it has been shown experimentally to react at very moderate temperatures (400 K) when annealed for an unknown time, and it is possible that it would also react at room temperature if annealed for long enough.

Gold Both the Au–Mo and Au–S binary systems show large miscibility gaps with limited solubility and no binary intermetallic phases.[158,159] No ternary phases are known. Therefore, gold must form a phase diagram with a tie line between MoS_2 and Au (Fig. 15). The Au–Mo–S phase diagram is categorized as MoS_2 dominant but could just as easily be categorized as Au dominant.

Lack of reactivity in the Au–MoS_2 system has been confirmed in multiple studies of Au atop both bulk and few-layer MoS_2.[33,160] In a 2013 study by Gong et al., a 2-nm Au film did not react upon deposition atop single-layer MoS_2, and did not fully wet the substrate.[26] Therefore, the phase diagram and experimental literature agree that Au does not react with MoS_2 at moderate temperatures.

DISCUSSION

MoS_2 Dominant Diagrams

Eight systems—Fe, Ru, Os, Rh, Pd, Pt, Cu, and Au—have room-temperature calculated diagrams which reflect MoS_2 dominance. Solid solubility could occur in some of these systems, but it is not addressed here for lack of information.

All of these elements are from groups 8 to 11 and have a *d* subshell that is more than half full (in contrast to groups 4 to 7, where no element has a *d* subshell containing more than five electrons). Some of these elements form ternary Chevrel phases, but they are absent from the reported ternary phase diagrams for moderate temperatures (Cu, Fe).

The singular feature of this diagram type is the tie line connecting MoS_2 with the transition metal, indicating that, for any ratio between the two, no new phases will form. However, some metals may intercalate, particularly at high temperatures (Ni, Pd).

Metal-Sulfide Dominant Diagrams

Mn and Cu (at 773 K) have metal-sulfide dominant diagrams. Each dominant sulfide has an energy of formation per atom ≤ -100 kJ/(mol of atoms) compared with -88 kJ/(mol of atoms) for MoS_2 at room temperature. Given these highly favored compounds, it is not surprising that they would form at the expense of MoS_2.

All of the experimental work examined reactions between excess MoS_2 and a limited supply of metal. Inspection of all of these ternary phase diagrams places such a sample in a three-phase region where Mo metal and a dominant metal sulfide (MnS or Cu_2S) are in equilibrium with MoS_2. When that reaction reaches completion, all of the metal will have been consumed in the formation of the appropriate sulfide, while liberating Mo metal. The excess MoS_2 will remain unreacted. This has been experimentally observed in both systems.

On the other hand, the reader should note that a sample with excess metal, as is the case when tens of nanometers of metal react with a few layers of MoS_2, will not result in the same equilibrium phases. In a sample containing excess metal, the equilibrium phases will be MnS, Mn_5Mo_4, and Mn; and Mo, Cu_2S, and Cu, respectively.

Solid Solution or Ternary Phase Dominant Phase Diagrams

For metals from groups 4 to 6, only three diagrams could be presented because a published ternary diagram was found (Ti, V, and W). The diagrams are all either solid solution or ternary phase dominant. Both W and V have a dominant ternary solid solution on their respective ternary phase diagrams.[61,78] Ti, on the other hand, displays a dominant ternary phase that is in equilibrium with MoS_2.[58]

Indeterminate Phase Diagrams

The presence of ternary phases prohibits us from calculating M–Mo–S ternary phase diagrams for M = Zr, Hf, Nb, Ta, Cr, Re, Co, Ni, and Ag, but reviewing the literature available for those systems can still inform future study.

Most of the early group transition metals (groups 4 to 7) form both layered binary dichalco-

genides and ternary Chevrel phases. Many form 2D layered TMDs that are being researched in their own right (TiS_2, ZrS_2, HfS_2, NbS_2, TaS_2, WS_2, and ReS_2).[2,161] The electronic properties of those compounds vary from semiconducting (TiS_2, ZrS_2, HfS_2, WS_2, MoS_2) to metallic (TaS_2, NbS_2, ReS_2).[162] Also, V, Nb, Ta, and W all show complete binary solid solubility with Mo.[70] Where experimental literature exists, all of these systems show evidence of reactivity.

Ternary phases are known or predicted to form in all of the group 4 to 7 systems, except Mn (ternary phase not reported), Tc (no literature), and W [which forms a $(Mo,W)S_2$ solid solution].

There is experimental evidence of reactivity at moderate temperatures in the Nb, Ta, Cr, and Ag systems. In contrast, in the Ni and Co systems, reaction was not seen below 600 K and 800 K, respectively, although it is unclear whether thermodynamic equilibrium was reached in either study.

CONCLUSIONS

The reaction products resulting from interaction between the transition metals and MoS_2 have been determined by calculating and compiling ternary phase diagrams, and then carefully comparing those results with the experimental literature on reactions. A few trends became evident:

1. MoS_2 dominant: Most of the late transition metal diagrams are dominated by MoS_2 and will likely not form additional binary intermetallic phases (M = Fe, Ru, Os, Rh, Pd, Pt, Cu, and Au).
2. M–S dominant: In a few systems, a very thermodynamically favored metal sulfide forms at the expense of MoS_2 (M = Mn, and Cu at 773 K).
3. Solid solution/ternary dominant: A solid solution or ternary phase is known to dominate a few published diagrams (M = Ti at 1573 K, V at 1373 K, and W at 773 K).
4. Indeterminate diagrams: In a few systems it was not possible to determine the exact equilibrium phases, but metal and MoS_2 have experimentally been shown to react at temperatures below 773 K in some of these systems, and therefore the diagram cannot be MoS_2 dominant (M = Nb, Ta, Cr, and Ag). Further experimentation in these systems is required to conclusively determine the equilibrium reaction products at moderate temperatures.

While the desired equilibrium products or diagram type depends on the intended application, knowledge of the anticipated equilibrium phases provides valuable insight to use when designing experiments in a variety of fields.

ACKNOWLEDGEMENTS

The authors would like to thank the National Science Foundation (DMR 1410334) for their support of this project.

APPENDIX

Appendix Table I.

Table I. Thermodynamic data used to calculate ternary phase diagrams

System	Phase	ΔH_f° kJ/(mol of atoms)	ΔS_f° J/(K·mol of atoms)	ΔG_f° kJ/(mol of atoms)	Refs.
Mo/S	MoS_2	−91.9	−10.0	−88.9	72
Mn	Mn_5Mo_4	−1[a]	*0*	−1	73
	MnS	−107.1	8.15	−109.5	72
	MnS_2	−74.6	1.303	−75.0	105
Fe	Fe_2Mo	−4.7	*0*	−4.7	73
	Fe_7Mo_6	*−3*	*0*	−3	73
	FeS	−50.1	0.505	−50.2	118
	$Fe_{11}S_{12}$	−49.9	3.08	−50.8	118
	$Fe_{10}S_{11}$	−49.9	3.238	−50.9	118
	Fe_9S_{10}	−50.0	3.04	−51.0	118
	Fe_7S_8	−50.4	2.62	−51.1	118
	FeS_2	−57.0	−12.8	−53.2	118
Ru	RuS_2	−68.6	−12.7	−64.8	72
Os	$OsMo_2$	*−17*	*0*	−17	73
	$OsMo_3$	*−19*	*0*	−19	73
	OsS_2	−49.0	−13.9	−44.8	72
Rh	Rh_3Mo	*−15*	*0*	−15	73
	RhMo	*−23*	*0*	−23	73
	$Rh_{17}S_{15}$	−44.4	*0*	−44.4	132
	Rh_3S_4	−51.1	−5.8	−49.4	72
	Rh_2S_3	−52.6	−6.7	−50.6	72
Pd	Pd_4S	−13.8	−0.6	−13.6	72
	$Pd_{16}S_7$	−25.22	*0*	−25.22	140
	PdS	−35.35	−6.70	−33.35	72
	PdS_2	−26.1	−4.7	−24.7	72
Pt	Pt_2Mo	*−34*	*0*	−34	73
	PtMo	*−42*	*0*	−42	73
	$PtMo_2$	*−35*	*0*	−35	73
	PtS	−41.6	−9.2	−38.8	72
Cu	Cu_2S	−26.81	5.735	−28.52	152
	$Cu_{1.95}S$	−27.06	4.98	−28.54	152
	$Cu_{1.75}S$	−27.64	3.07	−28.56	152
	CuS	−26.61	1.2	−26.97	152

[a]Assumed to be −1 kJ/(mol of atoms). See Mn section for further details.
Italicized ΔH_f° values indicate the use of Miedema's estimate as tabulated in de Boer.[73]
Italicized ΔS_f° values indicate where the entropy was approximated as zero.

REFERENCES

1. K.S. Novoselov, D. Jiang, F. Schedin, T.J. Booth, V.V. Khotkevich, S.V. Morozov, and A.K. Geim, *Proc. Natl. Acad. Sci. USA* 102, 10451 (2005).
2. S.Z. Butler, S.M. Hollen, L. Cao, Y. Cui, J.A. Gupta, H.R. Gutiérrez, T.F. Heinz, S.S. Hong, J. Huang, A.F. Ismach, E. Johnston-Halperin, M. Kuno, V.V. Plashnitsa, R.D. Robinson, R.S. Ruoff, S. Salahuddin, J. Shan, L. Shi, M.G. Spencer, M. Terrones, W. Windl, and J.E. Goldberger, *ACS Nano* 7, 2898 (2013).
3. S. McDonnell, R. Addou, C. Buie, R.M. Wallace, and C.L. Hinkle, *ACS Nano* 8, 2880 (2014).
4. S. Das, H.Y. Chen, A.V. Penumatcha, and J. Appenzeller, *Nano Lett.* 13, 100 (2012).
5. C. Gong, L. Colombo, R.M. Wallace, and K. Cho, *Nano Lett.* 14, 1714 (2014).
6. J.R. Chen, P.M. Odenthal, A.G. Swartz, G.C. Floyd, H. Wen, K.Y. Luo, and R.K. Kawakami, *Nano Lett.* 13, 3106 (2013).
7. R. Ganatra and Q. Zhang, *ACS Nano* 8, 4074 (2014).
8. M. Fontana, T. Deppe, A.K. Boyd, M. Rinzan, A.Y. Liu, M. Paranjape, and P. Barbara, *Sci. Rep.* 3, 1 (2013).
9. D.S. Tsai, D.H. Lien, M.L. Tsai, S.H. Su, K.M. Chen, J.J. Ke, Y.C. Yu, L.J. Li, and J.H. He, *IEEE J. Sel. Top. Quantum* 20, 3800206 (2014).
10. P. Stoyanov, R.R. Chromik, D. Goldbaum, J.R. Lince, and X. Zhang, *Surf. Coat. Technol. Lett.* 40, 199 (2010).
11. X.Z. Ding, X.T. Zeng, X.Y. Zeng, X.Y. He, and Z. Chen, *Surf. Coat. Technol.* 205, 224 (2010).
12. J.R. Lince, H.I. Kim, P.M. Adams, D.J. Dickrell, and M.T. Dugger, *Thin Solid Films* 517, 5516 (2009).
13. W. Chen, E.J.G. Santos, W. Zhu, E. Kaxiras, and Z. Zhang, *Nano Lett.* 13, 509 (2013).
14. B.G. Rao, H.S.S.R. Matte, P. Chaturbedy, and C.N.R. Rao, *ChemPlusChem* 78, 419 (2013).
15. T.F. Jaramillo, K.P. Jorgensen, J. Bonde, J.H. Nielsen, S. Horch, and I. Chorkendorff, *Science* 317, 100 (2007).
16. A. Splendiani, L. Sun, Y. Zhang, T. Li, J. Kim, C.Y. Chim, G. Galli, and F. Wang, *Nano Lett.* 10, 1271 (2010).
17. K.F. Mak, C. Lee, J. Hone, J. Shan, and T.F. Heinz, *Phys. Rev. Lett.* 105, 136805 (2010).
18. S. McDonnell, B. Brennan, A. Azcatl, N. Lu, H. Dong, C. Buie, J. Kim, C.L. Hinkle, M.J. Kim, and R.M. Wallace, *ACS Nano* 7, 10354 (2013).
19. W. Kautek, H. Gerischer, and H. Tributsch, *J. Electrochem. Soc.* 127, 2471 (1980).
20. K.K. Kam and B.A. Parkinson, *J. Phys. Chem.* 86, 463 (1982).
21. C.P. Lu, G. Li, J. Mao, L.M. Wang, and E.Y. Andrei, *Nano Lett.* 14, 4628 (2014).

22. H. Bergmann, B. Czeska, I. Haas, B. Mohsin, and K.H. Wandner, *Gmelin Handbook of Inorganic and Organometallic Chemistry, vol. Molybdenum Supplement B7*, 8th edn. (Springer, Berlin, 1992).
23. Y. Yoon, K. Ganapathi, and S. Salahuddin, *Nano Lett.* 11, 3768 (2011).
24. H. Zeng, J. Dai, W. Yao, D. Xiao, and X. Cui, *Nat. Nanotechnol.* 7, 490 (2012).
25. K.F. Mak, K. He, J. Shan, and T.F. Heinz, *Nat. Nanotechnol.* 7, 494 (2012).
26. C. Gong, C. Huang, J. Miller, L. Cheng, Y. Hao, D. Cobden, J. Kim, R.S. Ruoff, R.M. Wallace, K. Cho, X. Xu, and Y.J. Chabal, *ACS Nano* 7, 11350 (2013).
27. M.F. Cardinal, P.A. Castro, J. Baxi, H. Liang, and F.J. Williams, *Surf. Coat. Technol.* 204, 85 (2009).
28. L. Shi, C. Sun, and W. Liu, *Appl. Surf. Sci.* 254, 6880 (2008).
29. J. Nowotny, C.C. Sorrell, L.R. Sheppard, and T. Bak, *Catal. Hydrogen Energy* 30, 521 (2005).
30. J.D. Benck, T.R. Hellstern, J. Kibsgaard, P. Chakthranont, and T.F. Jaramillo, *ACS Catal.* 4, 3957 (2014).
31. J. Bonde, P.G. Moses, T.F. Jaramillo, J.K. Nørskov, and I. Chorkendorff, *Faraday Discuss.* 140, 219 (2009).
32. O.Y. Gutiérrez, S. Singh, E. Schachtl, J. Kim, E. Kondratieva, J. Hein, and J.A. Lercher, *ACS Catal.* 4, 1487 (2014).
33. J. Lince, D. Carré, and P. Fleischauer, *Phys. Rev. B* 36, 1647 (1987).
34. J.F. McGilp and I.T. McGovern, *J. Vac. Sci. Technol. B* 3, 1641 (1985).
35. J.F. McGilp, *J. Mater. Res.* 2, 516 (1987).
36. V.L. Kalikhman and Y.S. Umanskiĭ, *Sov. Phys. Uspekhi* 15, 728 (1973).
37. W. Jaegermann and H. Tributsch, *Prog. Surf. Sci.* 29, 1 (1988).
38. A.N. Zelikman, G.V. Indenbaum, M.V. Teslitskaya, and V.P. Shalankova, *Kristallografiya* 14, 795 (1969).
39. W.B. Jensen, *J. Chem. Educ.* 80, 952 (2003).
40. A.C. Lawson, *Mater. Res. Bull.* 7, 773 (1972).
41. R. Chevrel, M. Sergent, and J. Prigent, *J. Solid State Chem.* 3, 515 (1971).
42. A.M. Umarji, G.V.S. Rao, M.P. Janawadkar, and T.S. Radhakrishnan, *Solid State Commun.* 37, 1 (1981).
43. P. Vaqueiro, M.L. Kosidowski, and A.V. Powell, *Chem. Mater.* 14, 1201 (2002).
44. J. Guillevic, J.Y.L. Marouille, and D. Grandjean, *Acta Crystallogr. B* 30, 111 (1974).
45. K. Anzenhofer and J.J. De Boer, *Acta Crystallogr. B* B25, 1420 (1969).
46. R. Chevrel, M. Sergent, J.L. Meury, and D.T. Quan, *J. Solid State Chem.* 10, 260 (1974).
47. J. Guillevic, O. Bars, and D. Grandjean, *Acta Crystallogr. B* 32, 1338 (1976).
48. R. Chevrel, J. Guillevic, and M. Sergent, *C. R. Acad. Sci. Paris C* 271, 1240 (1970).
49. A. Oshima, E. Ike, H. Hinode, and M. Wakihara, *Thermochim. Acta* 191, 341 (1991).
50. A. Hårsta and E. Wennebo, *Acta Chem. Scand. A* 35, 227 (1981).
51. V.L. Kalikhman and A.A. Golubnichaya, *Sov. Phys. Crystallogr.* 28, 801 (1983).
52. A.M. Umarji, G.V.S. Rao, M.P. Janawadkar, and T.S. Radhakrishnan, *J. Phys. Chem. Solids* 41, 421 (1980).
53. R. de Jonge, T.J.A. Popma, G.A. Wiegers, and F. Jellinek, *J. Solid State Chem.* 2, 188 (1970).
54. J. Guillevic, M.O. Bars, and D. Grandjean, *J. Solid State Chem.* 7, 158 (1973).
55. A. Perrin, M. Sergent, and O. Fischer, *Mater. Res. Bull.* 13, 259 (1978).
56. M. Saeki and M. Onoda, *J. Less Common Met.* 135, L1 (1987).
57. M. Saeki and M. Onoda, *Chem. Lett.* 16, 1353 (1987).
58. H. Wada and M. Onoda, *J. Less Common Met.* 135, 205 (1987).
59. E.A. Marseglia, *Int. Rev. Phys. Chem.* 3, 177 (1983).
60. C.N.R. Rao and K.P.R. Pisharody, *Prog. Solid State Chem.* 10, 207 (1976).
61. H. Wada, M. Onoda, H. Nozaki, and I. Kawada, *J. Solid State Chem.* 63, 369 (1986).
62. V. Ivanovskaya, A. Zobelli, A. Gloter, N. Brun, V. Serin, and C. Colliex, *Phys. Rev. B* 78, 134104 (2008).
63. M. Kamaratos and C. Papageorgopoulos, *Solid State Commun.* 61, 567 (1987).
64. J.S. Zabinski and B.J. Tatarchuk, *Mater. Res. Soc. Symp. Proc.* 140, 239 (1988).
65. R. Chevrel, M. Sergent, and J. Prigent, *Mater. Res. Bull.* 9, 1487 (1974).
66. R. Baillif, K. Yvon, R. Flükiger, and J. Muller, *J. Low Temp. Phys.* 37, 231 (1979).
67. K. Yvon, A. Paoli, R. Flükiger, and R. Chevrel, *Acta Crystallogr. B* 33, 3066 (1977).
68. V.G.H. Moh, *Top. Curr. Chem.* 76, 107 (1978).
69. A. Hårsta, *J. Solid State Chem.* 57, 362 (1985).
70. T.B. Massalski (ed.), *Binary Alloy Phase Diagrams*, vol. 1–3, 2nd edn. (ASM International, Materials Park, 1990).
71. W.A. Brainard, *NASA Tech. Note* D–5141, 1 (1968).
72. O. Kubaschewski, C.B. Alcock, and P.J. Spencer, *Materials Thermochemistry*, 6th edn. (Pergamon, Oxford, 1993).
73. F.R. De Boer, R. Boom, W.C.M. Mattens, M.R. Miedema, and A.K. Niessen, *Cohesion in Metals: Transition Metal Alloys* (North-Holland Physics, Amsterdam, 1988).
74. A.R. Miedema, P.F. de Châtel, and F.R. de Boer, *Physica B* 100, 1 (1980).
75. M.W. Chase, *J. Phys. Chem. Ref. Data Monogr.* 9, 1 (1998).
76. R. Schmid-Fetzer, *J. Electron Mater.* 17, 193 (1988).
77. W.E. Liu and S.E. Mohney, *Mater. Sci. Eng. B* 103, 189 (2003).
78. V.G.H. Moh and G. Udubasa, *Chem. Erde* 35, 327 (1976).
79. M. Venkatraman and H. Newmann, *Binary Alloy Phase Diagrams, Chap. S-Sc (Sulfur-Scandium)* (ASM International, Materials Park, 1990), p. 3276.
80. L. Brewer and R.H. Lamoreaux, *Binary Alloy Phase Diagrams, Chap. Mo-Sc (Molybdenum-Scandium)* (ASM International, Materials Park, 1990), pp. 2660–2663.
81. L. Brewer and R.H. Lamoreaux, *Binary Alloy Phase Diagrams, Chap. Mo-Y (Molybdenum-Yttrium)* (ASM International, Materials Park, 1990), pp. 2686–2687.
82. M. Venkatraman and H. Newmann, *Binary Alloy Phase Diagrams, Chap. S-Y (Sulfur-Yttrium)* (ASM International, Materials Park, 1990), p. 3295.
83. G. Lütjering and J.C. Williams, Titanium, Chapter *Fundamental Aspects* (New York, 2007), pp. 15–52.
84. I.T. McGovern, E. Dietz, H.H. Rotermund, A.M. Bradshaw, W. Braun, W. Radlik, and J.F. McGilp, *Surf. Sci.* 152–153, 1203 (1985).
85. H. Okamoto, *J. Phase Equilib.* 24, 279 (2003).
86. H. Okamoto, *Binary Alloy Phase Diagrams, Chap. S-Zr (Sulfur-Zirconium)* (ASM International, Materials Park, 1990), pp. 3300–3301.
87. F.J. Mompean, J. Perrone, and M. Illemassène, *Chemical Thermodynamics of Zirconium*, vol. 8 (OECD Nuclear Energy Agency, Amsterdam, 2005).
88. T.B. Massalski, *Binary Alloy Phase Diagrams, Chap. Hf-S (Hafnium-Sulfur)* (ASM International, Materials Park, 1990), p. 2108.
89. L. Brewer and L.H. Lamoreaux, *Binary Alloy Phase Diagrams, Chap. Hf-Mo (Hafnium-Molybdenum)* (ASM International, Materials Park, 1990), pp. 2088–2089.
90. S. Fiechter and K. Eckert, *J. Cryst. Growth* 88, 435 (1988).
91. C. Mujica, J. Llanos, and O. Wittke, *J. Alloys Compd.* 226, 136 (1995).
92. A.V. Powell, A. McDowall, P. Vaqueiro, R.I. Smith, T. Ohtani, and Y. Okuya, *J. Mater. Chem.* 14, 3051 (2004).
93. W. Xiong, Y. Du, Y. Liu, B.Y. Huang, H.H. Xu, H.L. Chen, and Z. Pan, *CALPHAD* 28, 133 (2004).
94. T.B. Massalski, *Binary Alloy Phase Diagrams, Chap. Nb-S (Niobium-Sulfur)* (ASM International, Materials Park, 1990), pp. 2758–2762.

95. V. Raghavan, *J. Phase Equilib. Diff.* 27, 298 (2006).
96. P. Remmert, E. Fischer, and H.U. Hummel, *Z. Naturforsch. B* 49b, 1175 (1994).
97. S.R. Shatynski, *Oxid. Met.* 11, 307 (1977).
98. P.E.A. Turchi, L. Kaufman, and Z.K. Liu, *CALPHAD* 30, 70 (2006).
99. M. Venkatraman and H. Newmann, *Binary Alloy Phase Diagrams, Chap. Cr-S (Chromium-Sulfur)* (ASM International, Materials Park, 1990), pp. 1322–1326.
100. T.D. Durbin, J.R. Lince, and J.A. Yarmoff, *J. Vac. Sci. Technol. A* 10, 2529 (1992).
101. T.D. Durbin, J.R. Lince, S.V. Didziulis, D.K. Shuh, and J.A. Yarmoff, *Surf. Sci.* 302, 314 (1994).
102. A. Kumar and P.K. Ahluwalia, *Eur. Phys. J. B* 85, 186 (2012).
103. L. Brewer and R.H. Lamoreaux, *Binary Alloy Phase Diagrams, Chap. Mn-Mo (Manganese-Molybdenum)* (ASM International, Materials Park, 1990), pp. 2573–2575.
104. H.F. Franzen, *Binary Alloy Phase Diagrams, Chap. Mn-S (Manganese-Sulfur)* (ASM International, Materials Park, 1990).
105. D. Dilner, H. Mao, and M. Selleby, *CALPHAD* 48, 95 (2015).
106. J.R. Lince, T.B. Stewart, P.D. Fleischauer, J.A. Yarmoff, and A. Taleb-Ibrahimi, *J. Vac. Sci. Technol. A* 7, 2469 (1989).
107. L. Brewer and R. Lamoreaux, *Binary Alloy Phase Diagrams, Chap. Mo-Tc (Molybdenum-Technetium)* (ASM International, Materials Park, 1990).
108. H. Okamoto, *Binary Alloy Phase Diagrams, Chap. S-Tc (Sulfur-Technetium)* (ASM International, Materials Park, 1990), p. 3284.
109. P. Mao, K. Han, and Y. Xin, *J. Alloys Compd.* 464, 190 (2008).
110. K.K. Tiong, T.S. Shou, and C.H. Ho, *J. Phys. Condens. Matter* 12, 3441 (2000).
111. T.P. da Silva, M.O. Figueiredo, D. de Oliveira, J.P. Veiga, and M.J. Batista, *J. Miner. Mater. Charact. Eng.* 1, 207 (2013).
112. K.K. Tiong, P.C. Liao, C.H. Ho, and Y.S. Huang, *J. Cryst. Growth* 205, 543 (1999).
113. V. Raghavan, *Phase Diagrams of Ternary Iron Alloys, Chap. The Fe-Mo-S (Iron-Molybdenum-Sulphur) System* (Calcutta, 1988), pp. 174–187.
114. P.C. d'A Meneau and B. Boucher, *Acta Crystallogr. B* 33, 1495 (1977).
115. M. Kamaratos and C.A. Papageorgopoulos, *Surf. Sci.* 160, 451 (1985).
116. J.S. Zabinski, T. George, and B.J. Tatarchuk, *Thin Solid Films* 181, 485 (1989).
117. J.R. Lince, T.B. Stewart, M.M. Hills, P.D. Fleischauer, J.A. Yarmoff, and A. Taleb-Ibrahimi, *Surf. Sci.* 223, 65 (1989).
118. P. Waldner and A.D. Pelton, *J. Phase Equilib. Diff.* 26, 23 (2005).
119. H. Okamoto, *J. Phase Equilib.* 21, 572 (2000).
120. H. Okamoto, *J. Phase Equilib.* 12, 620 (1991).
121. H. Okamoto, *J. Phase Equilib.* 15, 455 (1994).
122. A. Taylor and N.J. Doyle, *J. Less Common Met.* 9, 190 (1965).
123. V.G. Kuznetsov, M.A. Sokolova, K.K. Palkina, and Z.V. Popova, *Inorg. Mater.* 1, 617 (1965).
124. K.P. Gupta, *J. Phase Equilib. Diff.* 25, 292 (2004).
125. J. Houserová, J. Vřešťál, and M. Šob, *CALPHAD* 29, 133 (2005).
126. V.L. Kalikhman, E.P. Gladchenko, A.G. Duksina, and A.G. Krupina, *Powder Metall. Met. Ceram.* 10, 475 (1969).
127. A. Mascaraque, L.M. de la Garza, and E.G. Michel, *Surf. Sci.* 482–485, 664 (2001).
128. J. Bulicz, L.M. de la Garza, and S. Fuentes, *Surf. Sci.* 365, 411 (1996).
129. J.R. Lince, D.J. Carre, and P.D. Fleischauer, *Langmuir* 2, 805 (1986).
130. H. Okamoto, *J. Phase Equilib.* 13, 108 (1992).
131. L. Kaufman, *CALPHAD* 14, 163 (1990).
132. O. Diéguez and N. Marzari, *Phys. Rev. B* 80, 214115 (2009).
133. E. Parthé, E. Hohnke, and F. Hulliger, *Acta Crystallogr.* 23, 832 (1967).
134. L. Brewer, L. Brewer, R.H. Lamoreaux, *Binary Alloy Phase Diagrams, Chap. Ir-Mo (Iridium-Molybdenum)* (ASM International, Materials Park, 1990), pp. 2328–2329.
135. S.H. Zhou, Y. Wang, C. Jiang, J.Z. Zhu, L.Q. Chen, and Z.K. Liu, *Mater. Sci. Eng. A* 397, 288 (2005).
136. P. Waldner and A.D. Pelton, *Z. Metallkd.* 95, 672 (2004).
137. W. Schramm, E. Gocke, and R. Schöllhorn, *Mater. Res. Bull.* 21, 929 (1986).
138. J.A. Rodriguez, *Polyhedron* 16, 3177 (1997).
139. C. Papageorgopoulos and M. Kamaratos, *Surf. Sci.* 164, 353 (1985).
140. A. Zubkov, T. Fujino, N. Sato, and K. Yamada, *J. Chem. Thermodyn.* 30, 571 (1998).
141. H. Okamoto, *J. Phase Equilib.* 13, 106 (1992).
142. G. Ghosh and G.B. Olson, *J. Phase Equilib.* 21, 32 (2000).
143. E. Perrot, A. Humbert, A. Piednoir, C. Chapon, and C.R. Henry, *Surf. Sci.* 445, 407 (2000).
144. L. Brewer and R.H. Lamoreaux, *Binary Alloy Phase Diagrams, Chap. Mo-Pt (Molybdenum-Platinum)* (ASM International, Materials Park, 1990), pp. 2650–2652.
145. H.F. Franzen, *Binary Alloy Phase Diagrams, Chap. Pt-S (Platinum-Sulfur)* (ASM International, Materials Park, 1990), pp. 3121–3125.
146. W.K. Hofmann, *J. Mater. Sci.* 23, 3981 (1988).
147. R.A. Simon, A.J. Ricco, D.J. Harrison, and M.S. Wrighton, *J. Phys. Chem.* 87, 4446 (1983).
148. D. Huang, L.L.Y. Chang, and C.R. Knowles, *J. Less Common Met.* 163, 281 (1990).
149. S. Yamamoto, K. Matsui, and M. Wakihara, *Mater. Res. Bull.* 18, 1311 (1983).
150. D.J. Chakrabarti, and D.E. Laughlin, *Bull. Alloy Phase Diagr.* 4, 254 (1983).
151. W.R. Cook Jr., (National Bureau of Standards (NBS) Special Publication, Gaithersburg, MD, 1972).
152. R.W. Potter, *Econ. Geol.* 72, 1524 (1977).
153. F. Grønvold, S. Stølen, E.F. Westrum Jr, and C.G. Galeas, *J. Chem. Thermodyn.* 19, 1305 (1987).
154. V.M. Glazov and A.S. Burkhanov, *Izv. Akad. Nauk. SSSR* 16, 565 (1980).
155. M.R. Baren, *Binary Alloy Phase Diagrams, Chap. Ag-Mo (Silver-Molybdenum)* (ASM International, Materials Park, 1990), pp. 59–60.
156. A. Souder and D.E. Brodie, *Can. J. Phys.* 49, 2565 (1971).
157. S.Y. Li, J.A. Rodriguez, J. Hrbek, H.H. Huang, and G.Q. Xu, *Surf. Sci.* 395, 216 (1998).
158. T.B. Massalski, H. Okamoto, and L. Brewer, *Binary Alloy Phase Diagrams, Chap. Au-Mo (Gold-Molybdenum)* (ASM International, Materials Park, 1990), pp. 395–397.
159. H. Okamoto and T.B. Massalski, *Binary Alloy Phase Diagrams, Chap. Au-S (Gold-Sulfur)* (ASM International, Materials Park, 1990), pp. 422–424.
160. C. Maurel, F. Ajustron, R. Péchou, G. Seine, and R. Coratger, *Surf. Sci.* 600, 442 (2006).
161. H.L. Zhuang and R.G. Hennig, *J. Phys. Chem. C* 117, 20440 (2013).
162. J.A. Wilson and A.D. Yoffe, *Adv. Phys.* 18, 193 (1969).